Available online at www.sciencedirect.com

SCIENCE DIRECT®

Sedimentary Geology 175 (2005) 391–414

Sedimentary Geology

www.elsevier.com/locate/sedgeo

Research paper

Integrated sequence stratigraphy: Facies, stable isotope and palynofacies analysis in a deeper epicontinental carbonate ramp (Late Jurassic, SW Germany)

M. Ruf[a], E. Link[b], J. Pross[b,c], T. Aigner[b,*]

[a]*Badley Ashton and Associates Ltd, Winceby House, Winceby, Horncastle, Lincolnshire, LN9 6PB, United Kingdom*
[b]*Institute of Geosciences, Tübingen University, Sigwartstr. 10, 72070 Tübingen, Germany*
[c]*Institute of Geology and Paleontology, Frankfurt University, Senckenberganlage 32-34, 60054 Frankfurt, Germany*

Received 10 May 2004; received in revised form 29 November 2004; accepted 17 December 2004

Abstract

Sequence stratigraphy in deeper water, epicontinental carbonates such as in the Upper Jurassic of southern Germany is difficult because the recognition of parasequences, sequences and sequence boundaries is impeded by the paucity in diagnostic sedimentological criteria or stratal surfaces. Using the "genetic stratigraphic" approach, and integrating facies, stable isotope (C, O) and palynofacies analysis two types of genetic depositional sequences can be discriminated: small-scale sequences are stacked into medium-scale sequences which may record a 400 kyr Milankovitch signal. The medium-scale sequences were correlated regionally using both gamma-ray logs and stable isotope records. Regional correlations show that the depocentres are controlled by underlying palaeotectonic elements (Late Palaeozoic troughs).

The rise/fall turnarounds of medium-scale sequences are marked by negative $\delta^{18}O$ peaks (temperature maxima) and reduced absolute palynoclast contents.

The fall/rise turnarounds are marked by positive $\delta^{18}O$ peaks (temperature minima) and high absolute palynoclast contents. The initiation and termination of sponge/microbial mounds show characteristic patterns: thrombolitic microbialites form during intervals of (1) reduced input of terrestrial palynomorphs interpreted as an increase in distality, (2) decreasing $\delta^{13}C$ trends interpreted to be related to decreasing nutrient supply and (3) decreasing $\delta^{18}O$ values interpreted as phases of warming and rising relative sea-level. In contrast, thrombolitic/stromatolitic microbialites were found to occur during phases of (1) increasing input of terrestrial palynomorphs interpreted as an increase in proximality, (2) increasing $\delta^{13}C$ values interpreted to reflect increasing terrestrial input and nutrient supply as well as increasing $\delta^{18}O$ values (interpreted as phases of cooling and relative

* Corresponding author. Tel.: +49 7071 2975923; fax: +49 7071 295727.
E-mail address: thomas.aigner@uni-tuebingen.de (T. Aigner).

0037-0738/$ - see front matter
doi:10.1016/j.sedgeo.2004.12.023

sea-level falls). Isotopic and palynofacies evidence suggests that bioherms were terminated by sudden input of nutrients during relative sea-level falls.

Sedimentological criteria were clearly not sufficient to delineate a robust sequence stratigraphic framework.

Keywords: Upper Jurassic; Sequence stratigraphy; SW Germany; Sponge/microbial bioherm; Gamma-ray log; Palynology

1. Introduction

Deeper ramp, epeiric carbonates, deposited below and up to storm wave base such as the Upper Jurassic of southern Germany are relatively uniform in lithological character (Pawellek and Aigner, 2003b). These deposits are poor in diagnostic sedimentological criteria commonly used for the identification of sequence boundaries or maximum flooding surfaces. Thus, when applying classical sequence stratigraphic methods, sequence boundaries are difficult to delineate. This paper attempts to document sequence stratigraphic patterns characteristic for deeper ramp carbonates. Facies, sequence, stable isotope and palynofacies analysis were integrated, resulting in an improved understanding of depositional processes and palaeoenvironmental changes.

2. Geological framework

The Upper Jurassic of southern Germany is subdivided by a well-defined framework of lithostratigraphy (Quenstedt, 1858; Gygi, 2000a,b), biostratigraphy (Hantzpergue et al., 1998; Gygi, 2000a,b; Schweigert, 2000; Baier and Schweigert, 2001) and sequence stratigraphy (Hardenbol et al., 1998; Sharland et al., 2001; Taylor et al., 2001; Colombié, 2002; Hug, 2003; Pawellek and Aigner, 2003a). This study covers the Late Jurassic Transversarium to Pseudomutabilis (lower part) ammonite zones (Fig. 1). In the submediterranean realm the Pseudomutabilis zone covers the same time interval as the Eudoxus zone. However, according to Baier and Schweigert (2001), the top of the Eudoxus zone in southern Germany does not correspond to the top of the Eudoxus zone in Great Britain and France. Instead, the uppermost part of the British and French Eudoxus zone correlates with the lower part of the Tethyan/submediterranean Beckeri zone. To avoid confusion, Baier and Schweigert (2001) suggest to replace the term Eudoxus zone by Pseudomutabilis zone in the Tethyan/submediterranean realm.

The lithostratigraphic subdivision for southern Germany dating back to Quenstedt (1858) is used here because it proved to be very practicable in outcrop, core and gamma-ray log analysis. Furthermore in the Swabian Basin the lithostratigraphic boundaries defined by Quenstedt (1858) correlate with biostratigraphic boundaries (Schweigert, personal communication 2004). To achieve the best fit between lithostratigraphic and biostratigraphic zonations Schweigert (personal communication, 2004) suggests to use the Mutabilis zone instead of the Acanthicum zone as the Mutabilis zone is more sharply defined. The Divisum and Mutabilis zones cover a time-span of about 1.1 Ma (Hardenbol et al., 1998; Fig. 1). This time-span was used to determine the duration of the identified sequences.

During the Late Jurassic, the study area was located in the deeper part of a gently inclined carbonate ramp, below and up to storm wave base (Pawellek and Aigner, 2003b). It was inundated by an epicontinental shelf sea marginal to the Tethys Ocean in the South (Meyer and Schmidt-Kaler, 1989; Ziegler, 1990). Towards the North, it was separated from the boreal realm by the Rhenish and the London–Brabant Massifs. Two shallow-water platforms flanked the study area: the Swiss Platform in the Southwest and the Franconian Platform in the East (Fig. 2). Between these two platforms the more basinal Swabian facies developed. The Swabian realm is characterized by two main lithofacies types: (1) well-bedded limestones alternating with marls and (2) sponge–microbial bioherms or mounds (Gwinner, 1976; Ziegler, 1977). Clastic input was mainly

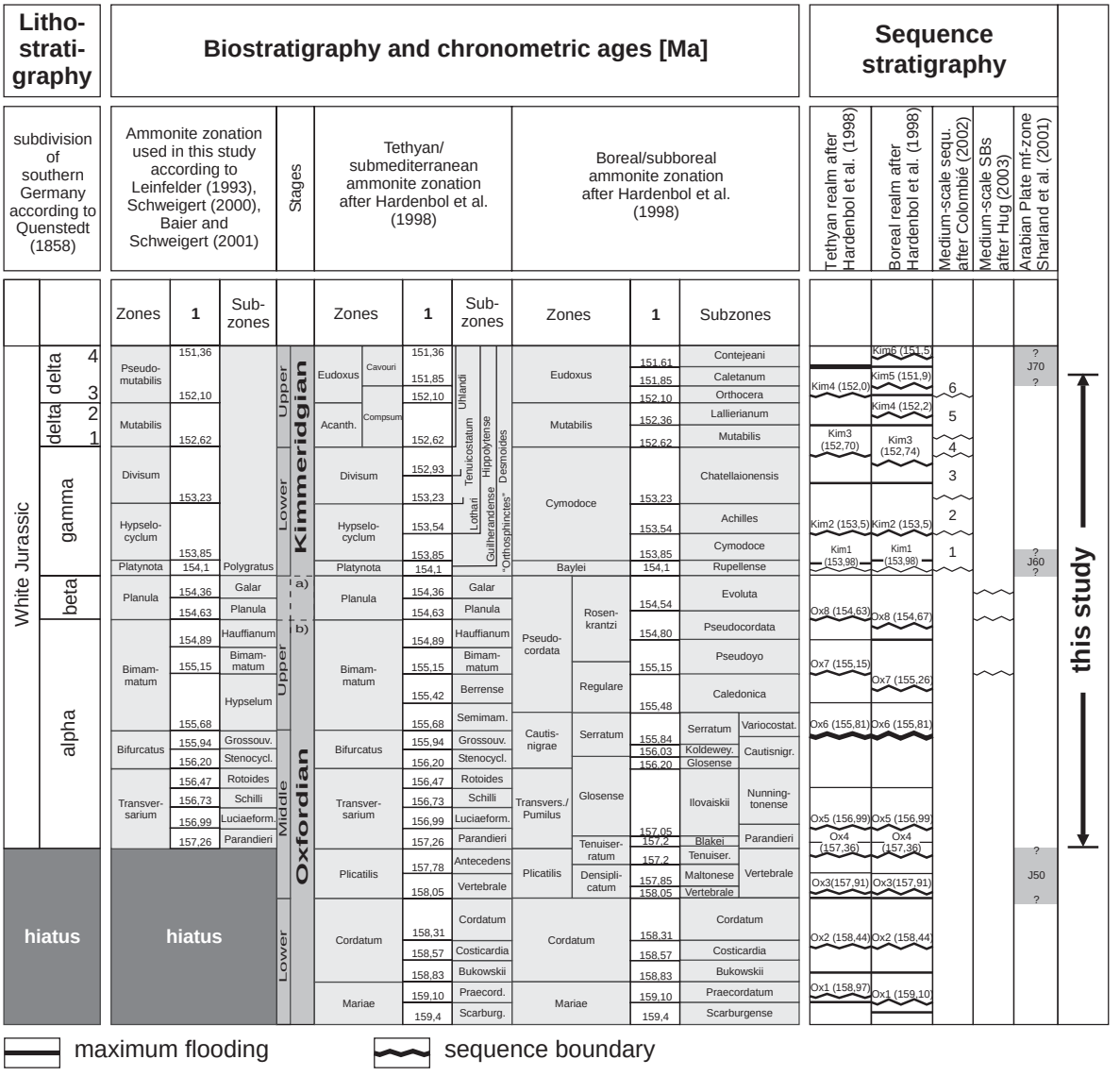

Fig. 1. Stratigraphic subdivision of the Upper Jurassic. The ammonite zonation according to Leinfelder (1993), Schweigert (2000) and Baier and Schweigert (2001) applies in the study area. However, the lithostratigraphic subdivision for southern Germany after Quenstedt (1858) is used in this study because it is very practicable in outcrop, core and gamma-ray log analysis and correlates with biostratigraphy (Schweigert, personal communication, 2004).

derived from the North (Gygi, 1986), probably from the Rhenish Massif (Meyer and Schmidt-Kaler, 1989). At least part of the carbonate mud deposited in the study area is supposed to be imported from the Swiss Platform (Pittet and Strasser, 1998; Pittet et al., 2000).

3. Material and methods

3.1. Sedimentology

This study is based on data from 97 sections (3 outcrops, 7 borehole cores, 3 outcrop gamma-ray

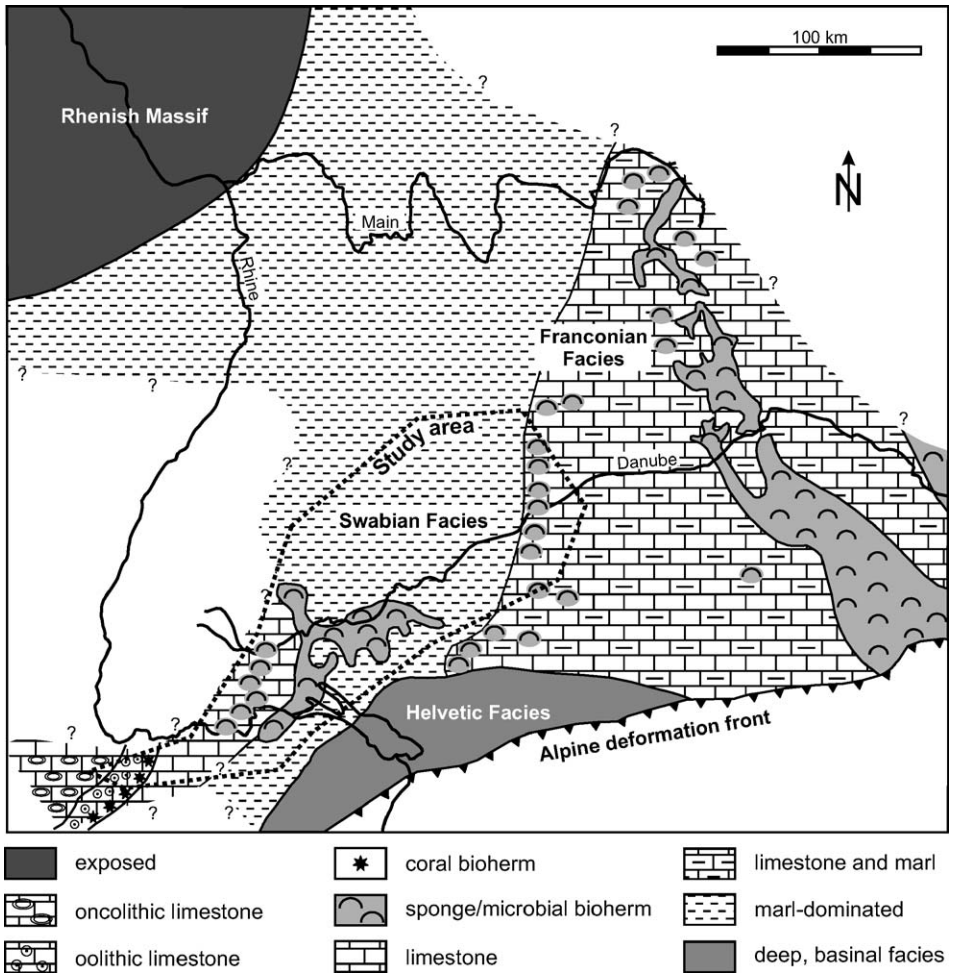

Fig. 2. Palaeogeography of southern Germany during the White Jurassic alpha (Upper Oxfordian) according to Meyer and Schmidt-Kaler (1989, 1990) and Gygi (1990). The study area is located in the Swabian Basin which is dominated by marly sediments (Swabian Facies). The Swabian basin is located in the deeper part of a gently inclined carbonate ramp marginal to the Tethys Ocean in the South. To the SW and the NE the Swabian Basin is bounded by two shallower water platforms: the Swiss platform and the Franconian platform. Clastic input was mainly derived from the Rhenish Massif in the North (Gygi, 1986; Meyer and Schmidt-Kaler, 1989).

logs and 91 borehole gamma-ray logs) in southern Germany and northern Switzerland (Fig. 3). Seven borehole cores and three outcrops were logged in detail. All cores were cut to allow continuous and semiquantitative logging. Microfacies analysis was carried out on 790 polished slabs and acetate peels. Out of this large database, the present paper has a particular focus on two borehole cores (Ro7324/B2 Auendorf and Ro7324/B3 Türkheim) and one outcrop (Plettenberg quarry; for locations see Fig. 3).

For gamma-ray log correlation 91 well logs and 3 outcrop gamma-ray logs were used. All gamma-ray measurements were recorded as counts per second (cps). The correlations were done by tracing characteristic successions of gamma-ray peaks. A prominent marker bed, the so-called “Glaukonitbank”, was chosen as datum for gamma-ray log correlation because it is regionally well traceable and considered to be isochronous within the limits of biostratigraphic resolution. The gamma-ray characteristics of the Glaukonitbank are well defined by a typical succession of peaks.

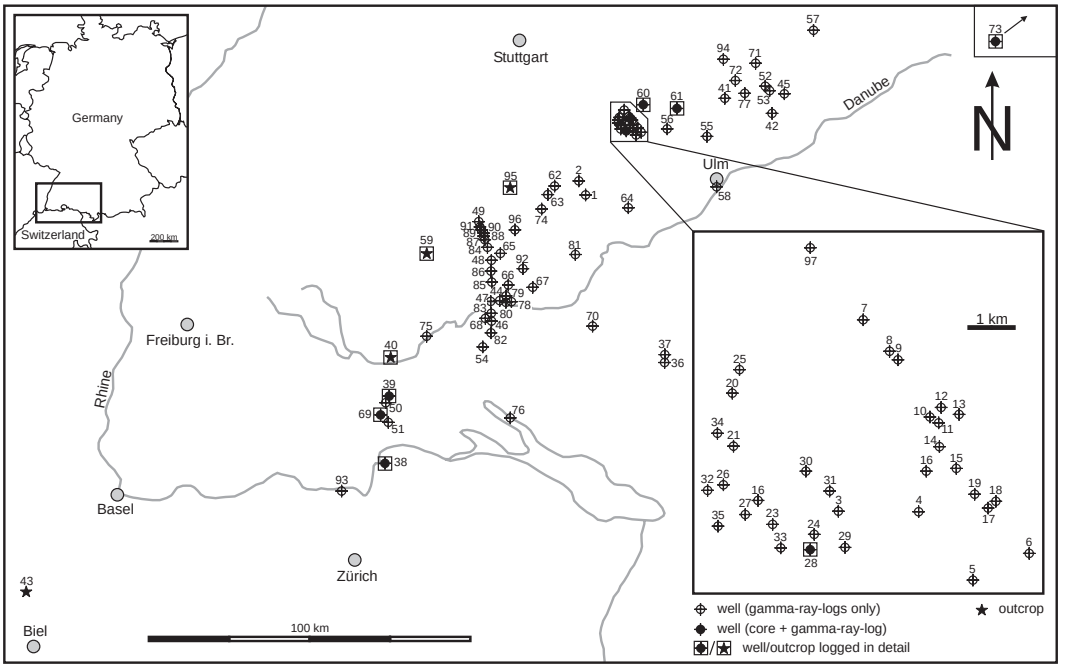

Nr.	Name	Coordinates (Gauss-Krüger)	
		Rechtswert	Hochwert
1	Alemannia B1	3533720	5359355
2	Alemannia B2	3531520	5363340
3	B 051	3546054	5378969
4	B 053	3547800	5378965
5	B 054	3548984	5377465
6	B 055	3550197	5378033
7	B 408	3546602	5383107
8	B 409	3547157	5382468
9	B 410	3547358	5382252
10	B 414	3548053	5381018
11	B 415	3548212	5380928
12	B 416	3548296	5381218
13	B 417	3548700	5381063
14	B 419	3548254	5380381
15	B 420	3548625	5379913
16	B 421	3547982	5379818
17	B 423	3549354	5379073
18	B 424/1	3549484	5379177
19	B 425	3549013	5379350
20	B 457	3543738	5381573
21	B 459	3543770	5380407
22	B 461	3544308	5379216
23	B 463	3544620	5378677
24	B 464	3545533	5378471
25	B 904	3543898	5382049
26	B 905	3543551	5379552
27	B 906	3544025	5378888
28	B 908	3545438	5378150
29	B 909	3546224	5378172
30	B 912	3545353	5379846
31	B 914	3545862	5379417
32	B 940	3543208	5379428
33	B 941	3544785	5378186
34	B 942	3543400	5380676
35	B 944	3543436	5378653
36	Bad Waldsee GB1	3557640	5309130
37	Bad Waldsee GB2	3557460	5311220
38	Benken	3473715	5278606
39	Espel KB1	3474342	5298443
40	Geisingen	3475130	5310340
41	Gerstetten GWM	3575400	5388320
42	Giengen-Burgberg GWM 21	3589706	5383549
43	Gorges du Pichoux	3366098	5240103
44	Gutenstein 1	3508183	5327217
45	Hölltal GWM	3593120	5389640
46	KB 4	3505411	5321160
47	KB 5	3505360	5327400
48	KB 6	3505566	5339512
49	KB 7	3501572	5350786

Nr.	Name	Coordinates (Gauss-Krüger)	
		Rechtswert	Hochwert
50	Litzental	3474063	5297301
51	Lohn	3474650	5290750
52	Mergelstetten GWM P1	3587601	5391623
53	Mergelstetten GWM P5	3588772	5390630
54	Meßkirch 1	3502800	5513600
55	Montenovo Pegel 1	3570190	5376660
56	Nellingen GWM	3558100	5378940
57	NeresheimB3 GWM1	3601988	5408508
58	Neu-Ulm TB	3573101	5361248
59	Plettenberg	3486049	5341603
60	RO 7324/B2	3550890	5386050
61	RO 7324/B3	3561100	5384980
62	RO 7621/B2	3524380	5361810
63	RO 7621/B5	3522510	5359240
64	RO 7623/B4	3546320	5355190
65	RO7720/B2	3508240	5341790
66	RO7820/B1	3510549	5332023
67	RO7821/B2	3517908	5331458
68	RO7920/B1	3503600	5322090
69	RO8217/B1	3472090	5293165
70	Saulgau TB3	3535700	5319900
71	Siebter Fuß GWM10	3584617	5398920
72	Steinheim-Stubental GWM	3578630	5393300
73	TreuMa	4432600	5426950
74	Trochtelfingen EB1	3520640	5355010
75	Tuttlingen GTB	3486117	5316419
76	Überlingen TB1	3511025	5292295
77	Ugenhof GWM	3581180	5389590
78	Unterschmeien 1	3511365	5326948
79	Unterschmeien 2	3509925	5328515
80	Unterschmeien 3	3509955	5327585
81	Upflamör 1	3530530	5341335
82	VB 17	3505411	5317851
83	VB 18	3505304	5323469
84	VB 19	3504285	5343436
85	VB 20	3505516	5333132
86	VB 21	3505425	5336442
87	VB 22	3503330	5345734
88	VB 23	3502896	5347065
89	VB 24	3502810	5347732
90	VB 25	3502202	5349047
91	VB 26	3501900	5349856
92	Veringenstadt1	3514805	5336917
93	Weiach	3460582	5270580
94	Wental GWM	3574780	5399900
95	Willmandingen	3511216	5361407
96	KB 18	3508400	5348980
97	B 404/1	3545382	5384702

Fig. 3. Study area and database. 97 sections (borehole cores, outcrops and gamma-ray logs) were analysed in this study.

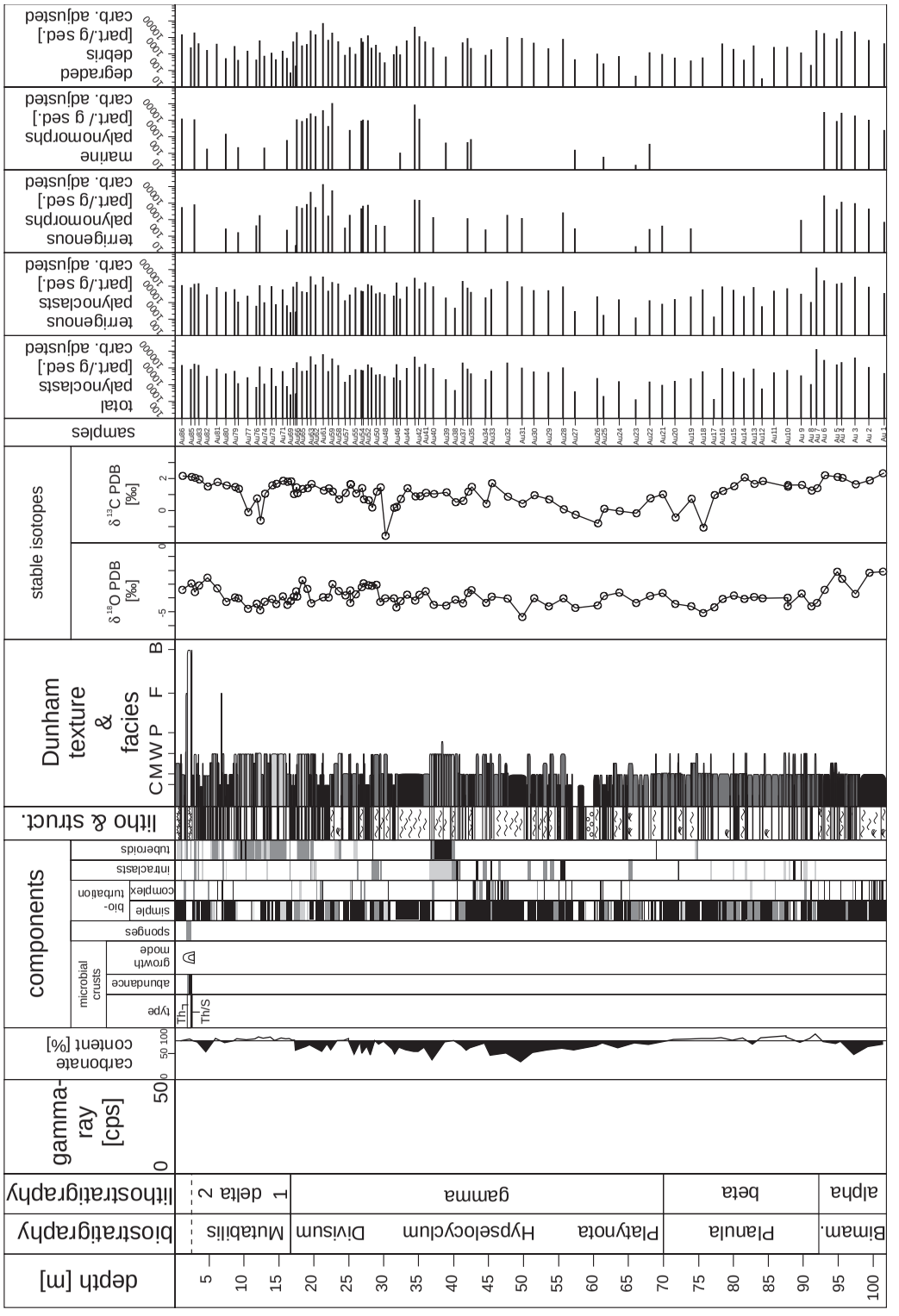

Fig. 4. Datasheet example. The data gained from each studied outcrop section and borehole core (here: well Ro7324/B2 Auendorf) was visualized in a datasheet as base for subsequent interpretations. The datasheets contain a gamma-ray log, a sedimentological log, stable isotope curves and the palynofacies data (see Fig. 7 for a key to the symbols). C—clay, M—mudstone, W—wackestone, P—packstone, F—floatstone, B—boundstone.

Gamma-ray logs are valuable tools for tracing litho-, sequence- and biostratigraphic boundaries (Taylor and Sellwood, 2002; Ruf and Aigner, 2004). In this study the gamma-ray logs were calibrated at litho- and biostratigraphic boundaries recognized in cores and correlated regionally. In this way a framework of time lines was established.

To discriminate marlstone from limestone in the gamma-ray log, the logs were normalized and core calibrated. A cut-off was set at 60% between the lowest and the highest gamma-ray peak. Peaks higher than 60% were regarded to represent marlstones, peaks lower than 60% limestones.

3.2. Stable isotope geochemistry

442 bulk rock samples were taken for stable isotope analysis of carbon and oxygen. Diagenetically not altered micrite areas were selected and powdered using an agate mill. After reacting the powder at 70 °C with phosphoric acid the isotopic composition of the resulting CO_2 was measured in an automated mode with a Gasbench II directly connected to a Finnigan Mat 252 mass spectrometre. All isotopic results are reported relative to the VPDB standard. The measurement precision is 0.1‰ for carbon and 0.2‰ for oxygen.

3.3. Palynofacies

Samples for palynofacies analysis were taken from the same rock specimens that were used for stable isotope analysis. Palynofacies samples were weighed and then processed using standard palynological techniques (Wood et al., 1996; Pross, 2001). 100 g of sediment for limestone and 50 g of sediment for marlstone were processed. In order to facilitate the calculation of absolute palynoclast abundance, the sample material was spiked with *Lycopodium* spore tablets (Stockmarr, 1971). No oxidation was applied to the sample material. The residues were sieved through an 11-μm nylon mesh. from each sample at least 300 palynoclasts were counted using a classification scheme based on Whitaker (1984), Boulter and Riddick (1986), Cole and Harding (1998) and Waterhouse (1995, 1999). The error induced during sample preparation, splitting and counting is assumed to be lower than 8%. Since absolute palynoclast abundances per gram bulk sediment in carbonate-dominated regimes strongly depend on the dilution by carbonate, a "carbonate adjustment" was performed for all palynofacies samples. First, absolute palynoclast abundances per gram bulk sediment were calculated using the *Lycopodium* marker spore method of Stockmarr (1971). Subsequently, "carbonate-adjusted" SOM (sedimentary organic matter) abundances were calculated following the equation:

$$A = N \cdot \frac{100}{C} \quad (1)$$

with A—carbonate-adjusted number of SOM clasts per gram of sediment, N—number of palynoclasts per gram of original sediment (including carbonate), and C—non-carbonate content of the sample in percent.

The following palynofacies parameters were used for interpretation: (1) all palynoclasts, (2) terrigenous palynoclasts (excluding terrigenous palynomorphs), (3) terrigenous palynomorphs (comprising pollen, spores, and freshwater algae), (4) marine palynomorphs (comprising dinoflagellate cysts, acritarchs, prasinophytes, other marine algae, and foraminifer test linings), and (5) degraded debris (representing palynoclasts of unknown origin).

Fig. 4 is an example of a datasheet summarizing all available information used for subsequent interpretation.

4. Results

4.1. Facies analysis

In this study 10 facies types were distinguished (Table 1). They are grouped into two main categories:

1. biohermal facies association
2. bedded limestone/marl facies association.

The biohermal facies association comprises:

a) Thrombolite/stromatolite limestones and thrombolite limestones: boundstones, mainly consist-

Table 1
Lithofacies types

Facies type	Number	Texture	Main components										Fabrics	Interpretation
			Thrombolites	Stromatolites	Silicious sponges	*Tubiphytes*	Terebelles	Brachiopods	Echinoderms	Peloids	Intraclasts	Tuberoids		
Sponge-thrombolite/ stromatolite limestones	1	B	○–●	◉–●	○–●	absent to ◉	absent to ◉			○	○	absent to ○	Massive appearance	Sponge/microbial bioherm
Sponge-thrombolite/ limestones	2	B	◉–●	absent to ○	○–●	absent to ◉	absent to ◉			○	○	absent to ○	Massive appearance	Sponge/microbial bioherm
Micritic sponge limestones	3a	F	absent to ○		◉–●			○						Sponge/microbial bioherm, inter-bioherm
Marly sponge limestones	3b	F marly matrix	absent to ○		◉–●			○						Sponge/microbial bioherm, inter-bioherm
Tuberoid debris limestones	4a	W - P			absent to ○	absent to ○	absent to ○			○	○	◉–●		Sponge/microbial bioherm debris
Marly tuberoid debris limestones	4b	W - P marly matrix			absent to ○	absent to ○	absent to ○			○	○	◉–●		Sponge/microbial bioherm debris
Coarse-grained bioherm debris limestones	5	(W - P), F			absent to ◉	absent to ○	absent to ○			○	○	◉–●	Often erosive base, (normal grading)	Episodic tempestites within sponge/microbial bioherms
Bioclast/intraclast debris limestones	6	W						○–◉	○–●	absent to ○	absent to ◉	absent to ○	Occasionally normal grading	Basinal facies, tempestites if graded
Well-bedded limestones	7	M						○	○	○	○	○	Well bedded, weak to intense bioturbation, intercalated marls	Basinal facies
Marls and marly limestones	8	M - clay						○	○			○	None to intense bioturbation	Basinal facies

○ = less abundant, ◉ = very abundant, ● = rock forming

Based on Dunham texture, main components and fabrics ten principal lithofacies types were distinguished (C—clay, M—mudstone, W—Wackestone, P—Packstone, F—Floatstone, B—Boundstone).

ing of silicious sponges and microbial thrombolitic and thrombolitic/stromatolitic crusts, forming bioherms with sizes ranging from several metres to several tens of metres in width and height.

b) Micritic sponge limestones and marly sponge limestones: sponge-rich floatstones, occurring within sponge-microbial bioherms or inter-biohermal areas.
c) Graded bioherm debris limestones: commonly graded wacke-, pack- or floatstones, composed of fragmented sponges and microbial crusts forming centimetre- to decimetre-thick layers within bioherms.
d) Tuberoid debris limestones and marly tuberoid debris limestones: wacke- or packstones, containing abundant sponge and microbial crust fragments, commonly forming fanlike sheets extending from sponge–microbial bioherms and interfingering with basinal facies (Fig. 5).

The bedded limestone/marl facies association comprises:

a) Bioclastic debris limestones: wackestones composed of reworked bioclasts and intraclasts, partly graded.
b) Well-bedded limestones: mudstones, forming decimetre-thick beds with thin intercalated marls (Fig. 6).
c) Marls and marly limestones: mostly mudstones with varying carbonate content.

4.2. Integrated sequence analysis: medium-scale sequences

The identification of sequences in this study is based on an integration of evidence derived from facies, isotope and palynofacies analysis.

Two main types of medium-scale sequences were distinguished based on rock composition: biohermal

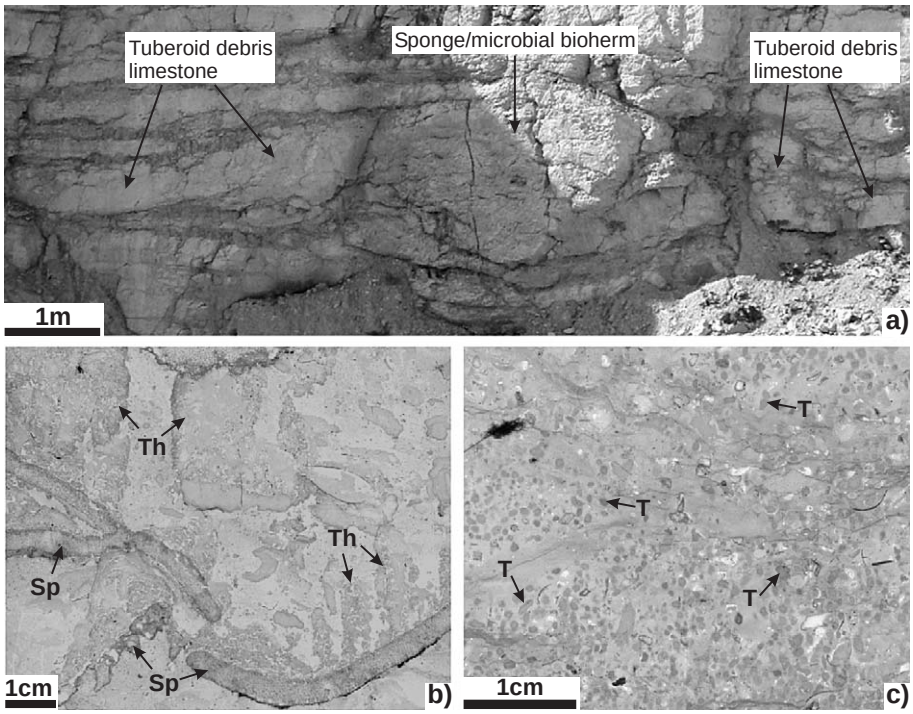

Fig. 5. Example for biohermal facies associations. (a) A small sponge/microbial bioherm from Plettenberg quarry is surrounded by fan-like wedges of tuberoid debris limestones extending from the bioherm. (b) Polished slab of thrombolite limestone with columnar growing thrombolites and plate-like sponges. (c) Polished slab of tuberoid debris limestone. Sp—sponge, Th—thrombolite, T—tuberoid.

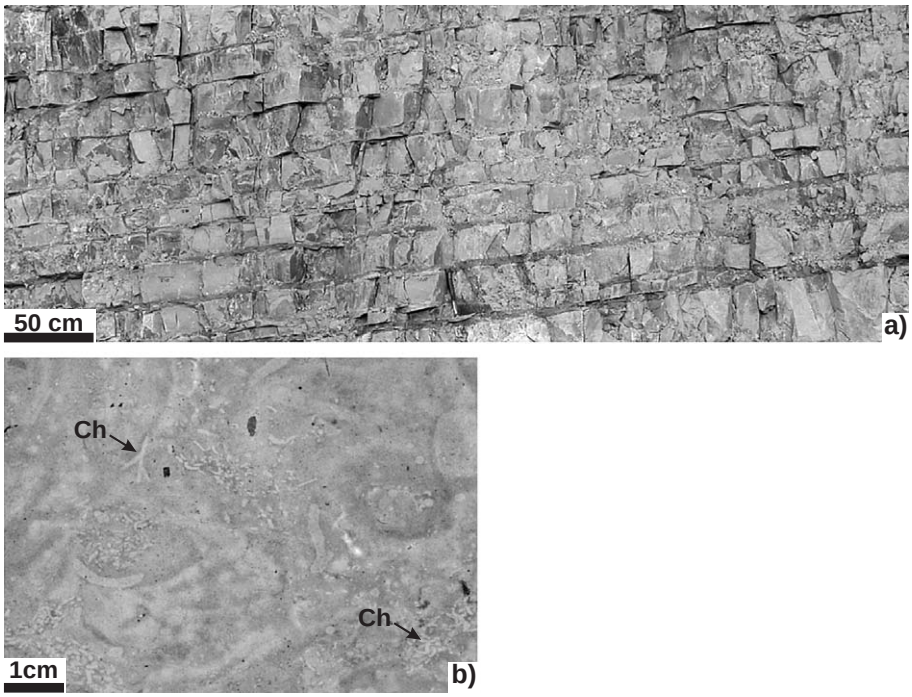

Fig. 6. Example for limestone/marl facies associations. (a) Well-bedded limestone from Plettenberg quarry. (b) Polished slab of heavily bioturbated well-bedded limestone. Ch—chondrites.

sequences and bedded limestone/marl sequences. Biohermal sequences are dominated by biohermal facies associations, bedded limestone/marl sequences are dominated by bedded limestone/marl facies associations.

4.2.1. Biohermal sequences

Medium-scale sequences 2 and 3 in Fig. 7 are typical examples of biohermal medium-scale sequences. Marls in the basal part are vertically succeeded by a tuberoid debris limestone. $\delta^{18}O$ values become increasingly positive within the tuberoid debris limestone. This trend correlates with an increase in absolute abundance of all palynoclast groups, especially of the terrigenous palynomorphs (medium-scale sequence 2 in Fig. 7). Above the tuberoid debris limestone thrombolite limestones developed. These thrombolite limestones are characterized by an increasingly negative $\delta^{18}O$ trend, a decreasing trend in $\delta^{13}C$ and decreasing absolute abundance in all palynofacies parameters. As the thrombolite limestones pass into thrombolite/stromatolite limestones, $\delta^{18}O$ and $\delta^{13}C$ values increase (medium-scale sequence 3 in Fig. 7). The absolute abundance of all palynofacies parameters increases upwards and displays a marked peak just above the thrombolite/stromatolite limestones. In this study a coupling of absolute abundance of terrestrial and marine palynomorphs was observed. The high absolute abundance of marine palynomorphs is nearly always linked with that of terrestrial palynomorphs (Figs. 4, 7 and 9).

4.2.2. Bedded limestone/marl sequences

Bedded limestone/marl sequences are composed of a variety of limestone facies types (e.g. well-bedded limestones, bioclast debris limestones or tuberoid debris limestones) and marls. Medium-scale sequence 1 in Fig. 9 is a typical example for a marl/tuberoid debris limestone medium-scale sequence.

The base is located within a thick tuberoid debris limestone. $\delta^{18}O$ values show a negative peak and the absolute palynoclast abundance is low. This is followed by a succession of tuberoid debris limestones and bioclast debris limestones with intercalated marls. Towards the top of this succession $\delta^{18}O$ values

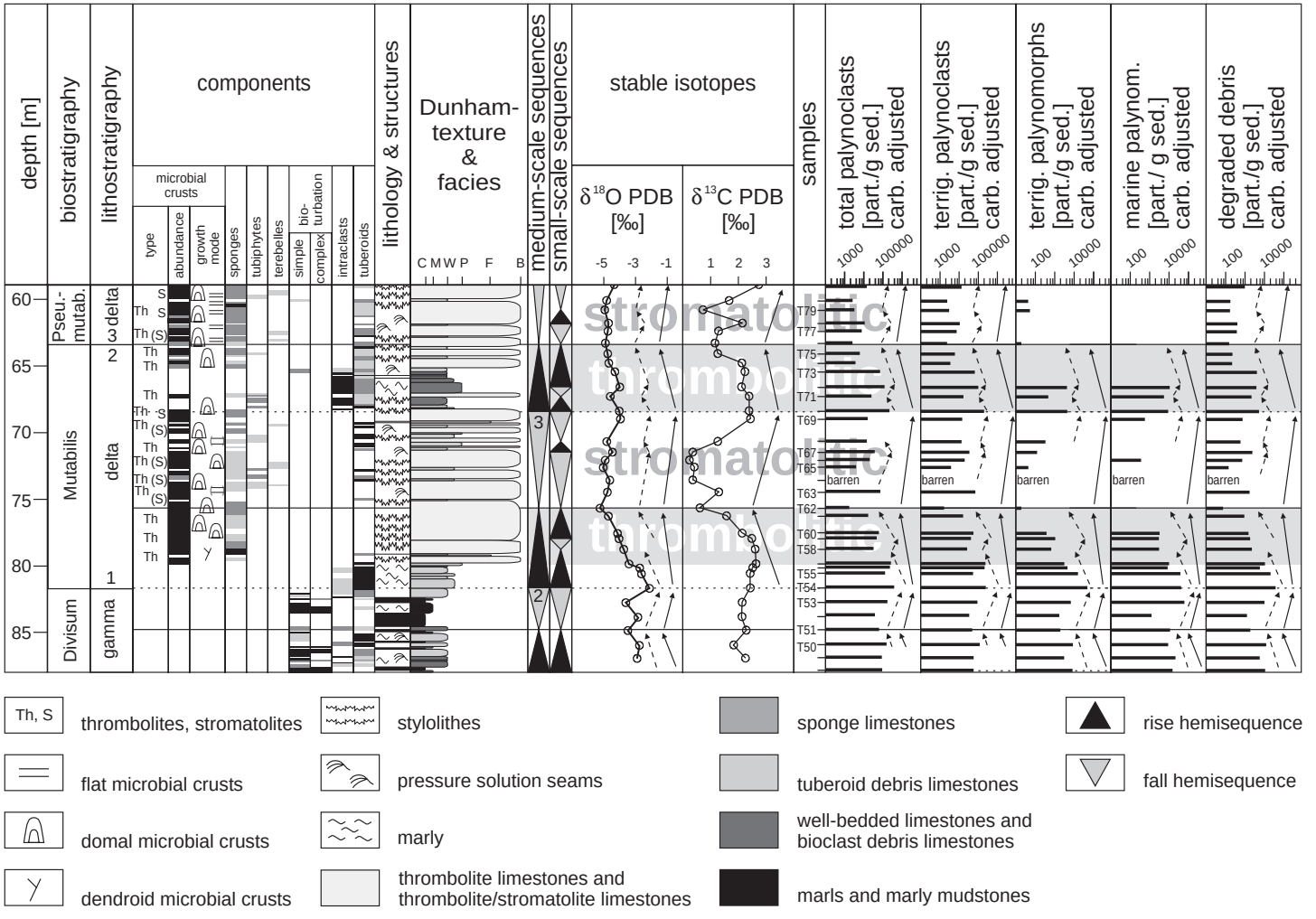

Fig. 7. Example for biohermal sequences from well Ro7324/B3 Türkheim. Medium-scale sequences are apparent in the trends in the oxygen isotope curve and absolute palynoclast abundance (black arrows). Increasing $\delta^{18}O$ values and increasing absolute palynoclast abundance are interpreted as fall hemisequences, decreasing $\delta^{18}O$ values and decreasing absolute palynoclast abundance are interpreted as rise hemisequences. Trends in $\delta^{18}O$ and palynofacies allowed to discriminate small-scale sequences (dotted arrows). Thrombolitic microbialites form during periods of decreasing absolute palynoclast abundance, decreasing $\delta^{13}C$ values and decreasing $\delta^{18}O$ values interpreted as phases of decreasing nutrient input and rising relative sea-level. Stromatolitic microbialites form during periods of increasing absolute palynoclast abundance, increasing $\delta^{13}C$ values and increasing $\delta^{18}O$ values interpreted as phases of increasing terrestrial input and nutrient supply as well as falling relative sea-level. C—clay, M—mudstone, W—wackestone, P—packstone, F—floatstone, B—boundstone.

become more positive and the absolute abundance of palynoclasts increases (Fig. 9). A thick marlstone covers the debris limestones, passing into a succession of bioclast debris and tuberoid debris limestones. This is accompanied by decreasing $\delta^{18}O$ values and decreasing absolute palynoclast abundance.

4.3. Correlation

Two correlation approaches were pursued in this study. Firstly, gamma-ray logs were core calibrated and correlated regionally to establish time lines within a frame defined by litho- and biostratigraphy. Secondly the medium-scale sequences identified in this study were correlated by means of carbon and oxygen isotope trends within the time-slices provided by gamma-ray log correlation.

A correlation of medium-scale sequences using only the gamma-ray log proved to be problematic as the turnarounds of medium-scale sequences do not always correspond to well-defined gamma-ray peaks but are often located at some point on the rising or falling part of the gamma-ray curve and are therefore hard to pick. The reason for that is that the turnarounds of medium-scale sequences are picked at pronounced oxygen isotope and palynoclast peaks and the sample resolution of isotope and palynofacies data is considerably lower than that of the gamma-ray logs.

4.3.1. Gamma-ray log correlation

Fig. 10a is a transect from the south-western margin of the Swabian Basin towards its north-eastern basin margin (line 1 in Fig. 10b). The sedimentary packages vary considerably in thickness. The thickest accumulations are documented in wells 86 to 62, corresponding to the central part of the Swabian basin. Towards the basin margins the succession becomes thinner.

Fig. 10c is a zoom into details of correlation line 1. In a thin stratigraphic interval the behaviour of individual marlstone packages and their corresponding gamma-ray log response was analysed. Marlstone packages thin from SW to NE, i.e. from basin to basin margin. Packages built by several individual gamma-ray peaks in the more basinal well 62 are represented by a reduced number of peaks in the more marginal wells. The clay content of some marlstones as represented by the gamma-ray log response is reduced considerably when approaching the basin margin.

Assuming similar compaction the marlstone thicknesses of the gamma-ray log parts in Fig. 10c were measured and expressed as percentage of the total thickness: well 62, 78%; well 28, 67%; well 8, 65%; well 60, 50% marlstones. This corresponds to a 30%-difference in marlstone content from basin to basin margin.

4.3.2. Isotope correlation

Stable isotopes, especially of carbon, are widely used for high-resolution correlation (Padden et al., 2002; Herrle et al., 2004). The medium-scale sequences recognized in this study could also be correlated by means of carbon and oxygen isotopes (Fig. 12). Oxygen isotopes correlate reasonably well over distances of more than 100 km. Carbon isotopes also correlate over short distances, whereas a high-resolution long-distance correlation is difficult.

5. Discussion and interpretation

5.1. Facies types

Graded bioherm debris limestones consist of in-situ reworked biohermal debris and are interpreted as reworked bioherm surfaces. Reworking probably occurred during episodic storm events (Pawellek and Aigner, 2003b).

Graded bioclastic debris limestones were commonly observed in more basinal settings and interpreted as turbidites (Ricken, 1985; Pawellek and Aigner, 2002).

Well-bedded limestones, marly limestones and marls are probably deposits of a low-energy quiet basinal environment.

5.2. General sequence concept

The classic EXXON sequence stratigraphic approach is based on the recognition of discrete surfaces, such as sequence boundaries or maximum flooding surfaces (Mitchum et al., 1977; Van Wagoner et al., 1988) allowing the discrimination of systems tracts. The fundamental units are asym-

metrical shallowing-upward (regressive) parasequences (Van Wagoner et al., 1990). In contrast, the fundamental building blocks recognized in the Upper Jurassic deeper ramp succession of southern Germany are more or less symmetrical (see also Braun, 1999; Pawellek and Aigner, 2003a). They consist of both a shallowing-upward (regressive) and a deepening-upward (transgressive) hemisequence. Contacts between sequences tend to be gradational rather than being defined by sharp stratal surfaces. Therefore, this study uses the approach of genetic stratigraphy as proposed by Wheeler (1964), Sonnenfeld (1996), Cross and Lessenger (1998) and Homewood et al. (2000).

Two hierarchies of sequences were distinguished: small-scale sequences, 3 to 7 m thick, are stacked into medium-scale sequences, 9 to 20 m thick (Fig. 7). The small-scale sequences show the same isotope and palynofacies trends as the medium-scale sequences (Figs. 7 and 8), but of a lower amplitude. The recognition of even smaller hierarchies of sequences, like the lime/marlstone bundles described by Munnecke and Westphal (2004) was not possible due to the sample resolution.

Time estimates for the medium-scale sequences recognized in this study suggest durations of about 400 kyr/sequence. The Divisum and Mutabilis ammonite zones cover a timespan of about 1.1 ma (Hardenbol et al., 1998) and contain 3 medium-scale sequences. The result is a timespan of roughly 400 kyr per medium-scale sequence taking into account the error of chronometric dating. Strasser et al. (2000) suggested that commonly depositional sequences are formed by the 400 kyr eccentricity cycle and controlled by climatically induced sea-level changes. A link between medium-scale sequences and climatic (temperature) changes was documented using the $\delta^{18}O$ curve (see below).

The recognition of sequences in this study is based on an integration of facies, isotopic and palynofacies evidence. Previous studies by Pawellek (2001) and Pawellek and Aigner (2003a) could only rely on sedimentological criteria for the definition of sequence turnarounds, resulting in a different sequence framework. The multi-proxy approach used here leads most likely to a more robust sequence delineation compared to the purely sedimentologic definition in previous studies.

5.3. Biohermal sequences

Besides facies and palynofacies criteria the oxygen isotope record is a major proxy used for interpretation of the sequences recognised in this study.

The oxygen isotope composition of sea water is influenced by many factors. Besides temperature, salinity can have a major influence on $\delta^{18}O$ (Bartolini et al., 2003). Meteoric water has significantly lower $\delta^{18}O$ values than sea water and freshwater input may therefore be the cause of negative excursions in the oxygen isotope record.

Comparing the oxygen isotope record with the palynofacies dataset, it is suggested that freshwater input into the Swabian Marl Basin from surrounding land masses is not the main cause for the observed $\delta^{18}O$ trends. Intervals of high terrestrial input are characterised by enhanced absolute abundances of terrigenous palynoclasts. Instead of having more negative $\delta^{18}O$ values as would be expected as a result of influx of isotopically light freshwater, these intervals are characterised by a positive excursion in the oxygen isotope record. Furthermore the Late Jurassic climate in Europe is dominated by a trend to increasing aridity from the Oxfordian throughout the Kimmeridgian (Abbink et al., 2001). General circulation model simulations for the Kimmeridgian also predict at least seasonally arid conditions in Europe (Valdes and Sellwood, 1992; Valdes, 1993; Valdes et al., 1995). Significantly increased runoff over longer time intervals, which would be necessary to explain major negative trends in the oxygen isotope record are therefore not compatible with the climatic boundary conditions during the Kimmeridgian in central Europe.

Generally, $\delta^{18}O$ values decrease with increasing sea water CO_3^{2-} -ion concentration. Decreasing alkalinity may therefore lead to more negative $\delta^{18}O$ (Elderfield et al., 1999).

However, decreasing $\delta^{18}O$ values were often observed in intervals characterised by thrombolite-dominated sponge/microbial bioherm growth (Fig. 7). According to Kempe et al. (1996) and Wood (2001), mud mound and microbialite formation are favoured by high pH. Therefore it can be assumed that alkalinity was not a major factor controlling the oxygen isotope signature.

Temperature variations are therefore considered as the most important factor controlling the $\delta^{18}O$ signal

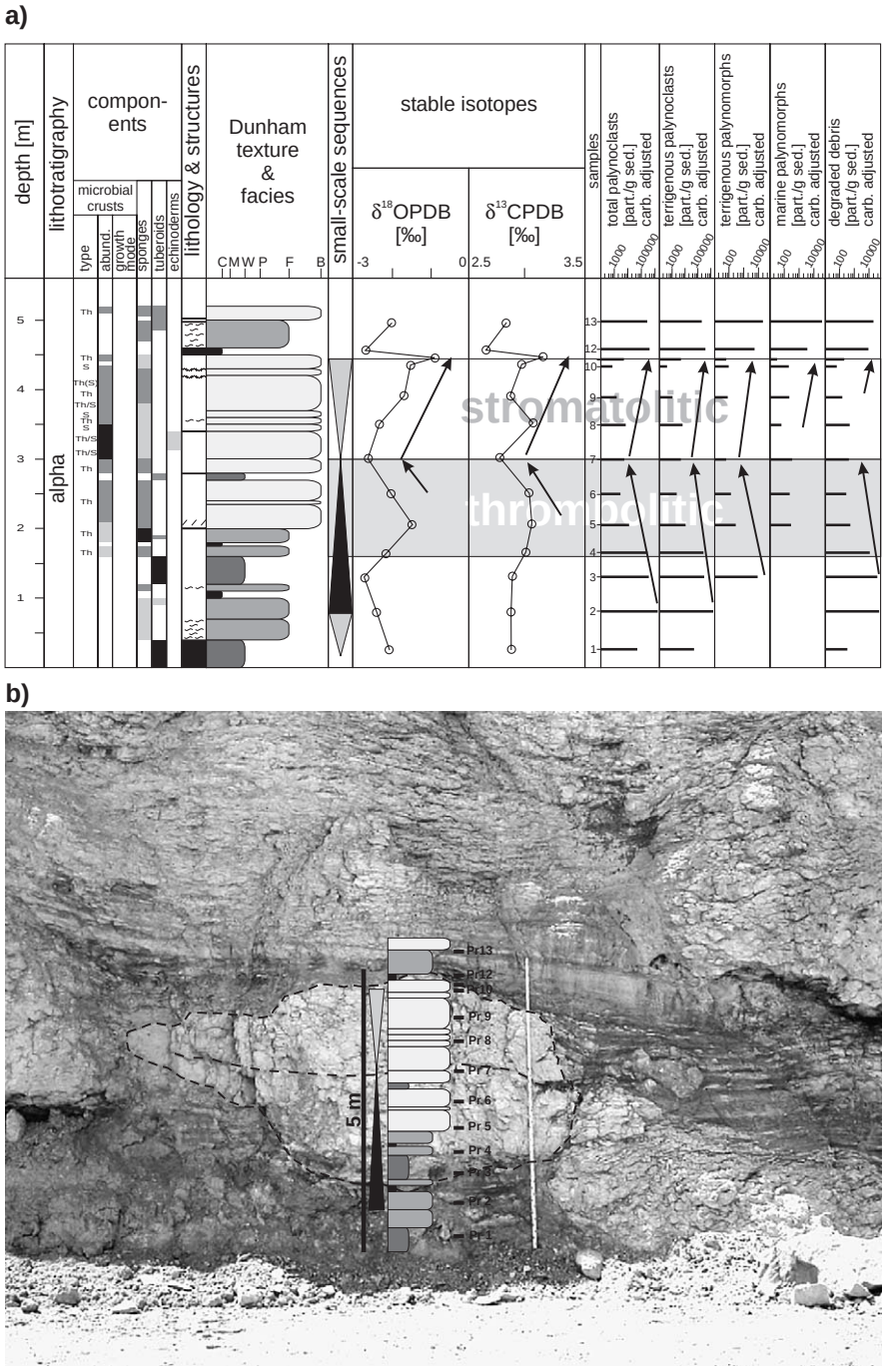

Fig. 8. Biohermal small-scale sequence in outcrop (Plettenberg Quarry). (a) Decreasing $\delta^{18}O$ and $\delta^{13}C$ values and decreasing absolute palynoclast abundance reflect periods of thrombolite development, interpreted as a rise hemisequence. Increasing $\delta^{18}O$ and $\delta^{13}C$ values and increasing absolute palynoclast abundance reflect periods of stromatolite development, interpreted as a fall hemisequence. (b) Thrombolite facies develops in periods of bioherm expansion, thrombolite/stromatolite facies develops during periods of bioherm retreat. See Fig. 7 for a key to the symbols. C—clay, M—mudstone, W—wackestone, P—packstone, F—floatstone, B—boundstone.

and thus the $\delta^{18}O$ curve is used here as a tool for estimating relative changes in temperature.

A positive $\delta^{18}O$ shift is interpreted as a trend towards cooler water temperatures, whereas a negative shift is regarded to express a temperature increase (Epstein et al., 1953; Craig, 1965; Weissert and Erba, 2004). Cooler climates are often periods with lower sea-level, warmer climates are often periods with higher sea-level (Sandberg, 1983; Abbink et al., 2001). Positive $\delta^{18}O$ excursions (e.g. in the tuberoid limestone part of biohermal medium-scale sequence 2 in Fig. 7) are therefore interpreted to depict a fall in relative sea-level. This interpretation is supported by the palynofacies data. The high absolute abundance of all palynoclast groups and especially of terrestrial palynomorphs suggests a relative sea-level fall (Waterhouse, 1995; Bombardiere and Gorin, 2000; Tyson and Follows, 2000). Vice versa, a decrease in absolute palynoclast abundance, especially in terrestrial palynomorphs, and a negative shift of $\delta^{18}O$ in the thrombolitic limestones are interpreted as relative sea-level rises. A positive $\delta^{18}O$ peak associated with a peak in absolute palynoclast abundance is interpreted as the fall/rise turnaround of medium-scale sequences (e.g. medium-scale sequence 2 in Fig. 7).

Thrombolites are associated with transgression or low energy deeper water conditions according to many authors (Keupp et al., 1993; Leinfelder, 1993; Leinfelder et al., 1993, 1996; Dromart et al., 1994; Schmid, 1996). They were observed down to water depths of several hundreds of metres (Schmid, 1996). Increasing water depth during thrombolite limestone formation is indicated by decreasing absolute abundance of terrestrial palynomorphs. This palynofacies pattern suggests increasingly distal conditions and therefore a rise in relative sea-level (Waterhouse, 1995; Bombardiere and Gorin, 2000; Tyson and Follows, 2000). Progressively lighter values of $\delta^{18}O$ values are probably due to an increase in temperature favouring a relative sea-level rise. Thrombolites only tolerate rather low sedimentation rates (Leinfelder et al., 1994, 1996). Pittet and Strasser (1998) and Pittet et al. (2000) suggest low export of carbonate mud from the Swiss platform towards the deeper ramp during phases of early transgression. In such periods carbonate sedimentation rates in the Swabian Basin are regarded to be low and thrombolite growth is favoured.

Removal of isotopically light carbon from surface waters due to increased organic productivity is supposed to be the cause for a positive $\delta^{13}C$ shift (e.g. in the basal part of the thrombolite limestone in medium-scale sequence 2; Fig. 7; Berger and Vincent, 1986; Marshall, 1992). High organic productivity in surface waters is also reflected in the palynofacies record by high amounts of marine palynomorphs (Waterhouse, 1995; Bombardiere and Gorin, 2000; Tyson and Follows, 2000). Degradation of organic matter raining down from higher parts of the water column may consume the oxygen on the sea floor (Huc, 1988). A bloom of planktic organisms in surface waters may therefore cause occasional oxygen depletion in bottom waters which is assumed to have been favourable for thrombolite development (Rehfeld, 1996; Leinfelder, 2001).

To explain the in-phase variation of the absolute abundance of terrestrial and marine palynomorphs (Figs. 4, 7 and 9) it is likely that marine productivity was boosted by high influx of nutrients from land areas, with the latter being reflected by high absolute abundance of terrestrial palynomorphs (Harris and Tocher, 2003; McCarthy et al., 2004). High nutrient levels are known to disturb or even prevent carbonate production on the shallow platform (Hallock and Schlager, 1986). The result is a reduced export of carbonate mud from the platform and low carbonate sedimentation rates on the deeper ramp which, in turn, favour thrombolite formation. According to Whalen et al. (2002), thrombolites seem to be associated with environmental change or biotic crisis in carbonate systems.

The most negative $\delta^{18}O$ peak in combination with a low absolute abundance in all palynofacies parameters can be regarded to indicate maximum flooding and therefore marks a rise/fall turnaround (see the medium-scale sequence2/medium-scale sequence3 rise/fall turnaround in Fig. 7). The $\delta^{13}C$ curve shifts towards more negative values when approaching the rise/fall turnaround. This negative excursion is considered to depict a decrease of organic productivity in surface waters probably caused by reduced nutrient availability (see also Weissert et al., 1998). This is concordant with the observations of Pittet and Mattioli (2002) who analysed calcareous nannofossils from the Oxfordian

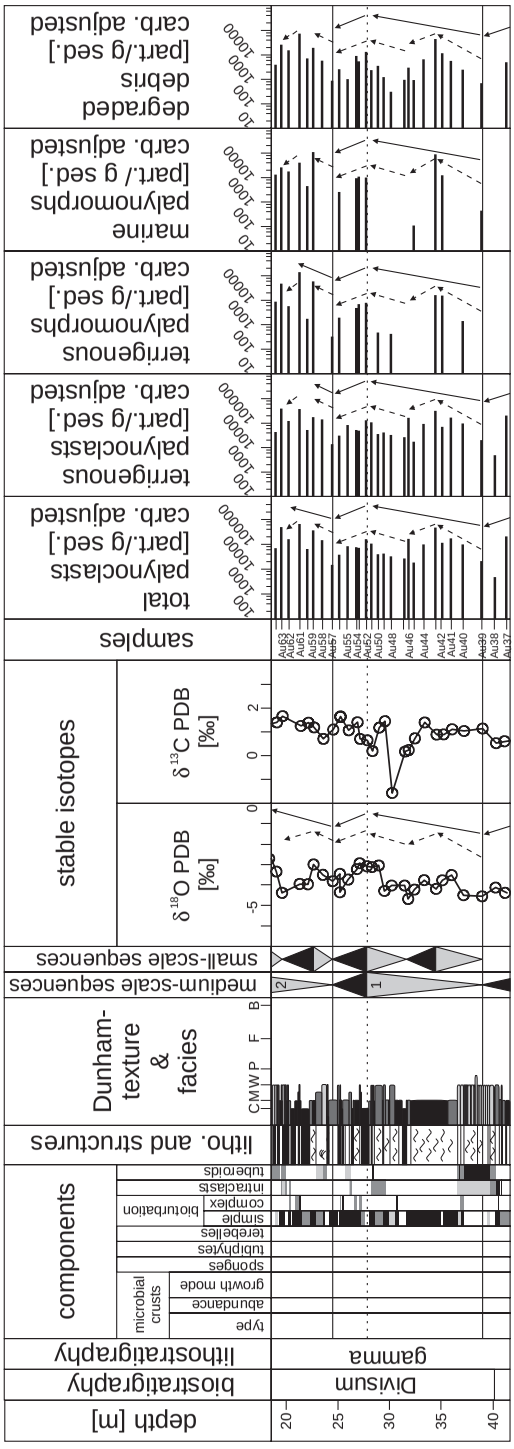

Fig. 9. Example for bedded limestone/marl sequences from well Ro7324/B2 Auendorf. Trends in the oxygen isotope record and absolute palynoclast abundance (black arrows) define medium-scale sequences. Increasing $\delta^{18}O$ values and increasing absolute palynoclast abundance are interpreted as fall hemisequences, decreasing $\delta^{18}O$ values and decreasing absolute palynoclast abundance are interpreted as rise hemisequences. Trends in $\delta^{18}O$ and palynofacies allowed to discriminate small-scale sequences (dotted arrows). See Fig. 7 for a key to the symbols. C—clay, M—mudstone, W—wackestone, P—packstone, F—floatstone, B—boundstone.

of southern Germany and describe an in-phase coupling of relative sea-level rise and reduced nutrient availability.

Above the rise/fall turnaround the first stromatolites were observed (Fig. 7). Stromatolites are commonly regarded as indicators for shallower water and more tolerant towards higher sedimentation rates (Golubic and Knoll, 1993; Defarge et al., 1994; Rehfeld, 1996; Schmid, 1996). $\delta^{18}O$ values increase towards the top of the thrombolite/stromatolite limestone unit. This trend is interpreted as cooling and relative sea-level fall. The increasing absolute abundance of terrestrial palynomorphs also indicates falling sea-level (Waterhouse, 1995; Bombardiere and Gorin, 2000; Tyson and Follows, 2000). Towards the top reworking increases suggesting episodic high energy storm events caused by a sea-level drop (Pawellek and Aigner, 2003b).

Increased hydrodynamic energy during lowering of sea-level might result in improved oxygenation obstructing thrombolite growth (Leinfelder, 2001). The initial stages of thrombolite/stromatolite limestone formation are dominated by low values of $\delta^{13}C$ and low absolute palynoclast abundance. Both facts suggest low organic productivity and low nutrient influx (Waterhouse, 1995; Weissert et al., 1998; Bombardiere and Gorin, 2000; Tyson and Follows, 2000).

The positive $\delta^{18}O$ peak and the sudden increase in absolute palynoclast abundance is interpreted as a fall/rise turnaround (see medium-scale sequence 3 in Fig. 7). This is combined with a sharp positive shift in $\delta^{13}C$, probably caused by a very sudden input of nutrients during low relative sea-level. Bioherm development terminates at this fall/rise turnaround. The bioherm community was probably smothered by high terrigenous clastic and nutrient input.

Fig. 8 is an outcrop example of an small-scale biohermal sequence. The rise to fall turnaround is characterized by a negative $\delta^{18}O$ peak and low palynoclast content. Pure thrombolite limestones are confined to a period of relative sea-level rise as indicated by oxygen isotopes and palynofacies record. Thrombolite/stromatolite limestones developed during a period of relative sea-level fall. Outcrop bioherm geometry suggests that the thrombolite facies represents periods of bioherm expansion while the thrombolite/stromatolite facies show a retreating bioherm (Fig. 8).

The results discussed above suggest that thrombolite growth is triggered during relative sea-level rise by initially high but decreasing nutrient influx, low sedimentation rates and presumably occasionally lowered oxygen level. Thrombolites preferentially form up to maximum transgression when nutrient influx is at a minimum. During the subsequent sea-level fall nutrient availability and organic productivity increase again giving rise to mixed thrombolite/stromatolite communities. The maximum relative sea-level fall and bioherm termination are marked by a sudden increase in terrestrial input of clay and palynomorphs. This increase in nutrient influx at the same time boosted marine productivity. Nutrient availability seems to be a major factor for the evolution of deeper water sponge–microbial bioherms in the Upper Jurassic of SW Germany.

5.4. Bedded limestone/marl sequences

The delineation of bedded limestone/marl sequences is strongly based on the interpretation of oxygen isotope and palynofacies data, as sedimentary facies does not provide clear evidence suitable for the recognition of medium-scale sequences.

Decreasing absolute palynoclast abundance and negative trends in $\delta^{18}O$ are interpreted to indicate a rising relative sea-level while increasing absolute palynoclast abundance and positive trends in $\delta^{18}O$ are regarded to indicate a falling relative sea-level (see above). Pronounced negative $\delta^{18}O$ peaks and relatively low absolute palynoclast abundance, especially of terrestrial palynomorphs (e.g. at the base of medium-scale sequence 1; Fig. 9) are interpreted to indicate maximum flooding expressed in a rise/fall turnaround. In contrast a positive shift in $\delta^{18}O$ and increased absolute palynoclast abundance (e.g. in the top of the tuberoid and bioclast debris limestone succession of medium-scale sequence 1; Fig. 9) are interpreted to represent a fall/rise turnaround. The early rise, directly above the fall/rise turnaround consists of a thick marlstone. Many units containing very high amounts of clay are in this study interpreted as deposits of “lowstands” and early relative sea-level rises. Pittet and Strasser (1998) and Pittet et al. (2000) proposed a model connecting sea-level changes affecting the shallow Swiss platform with associated sediments of the deeper shelf.

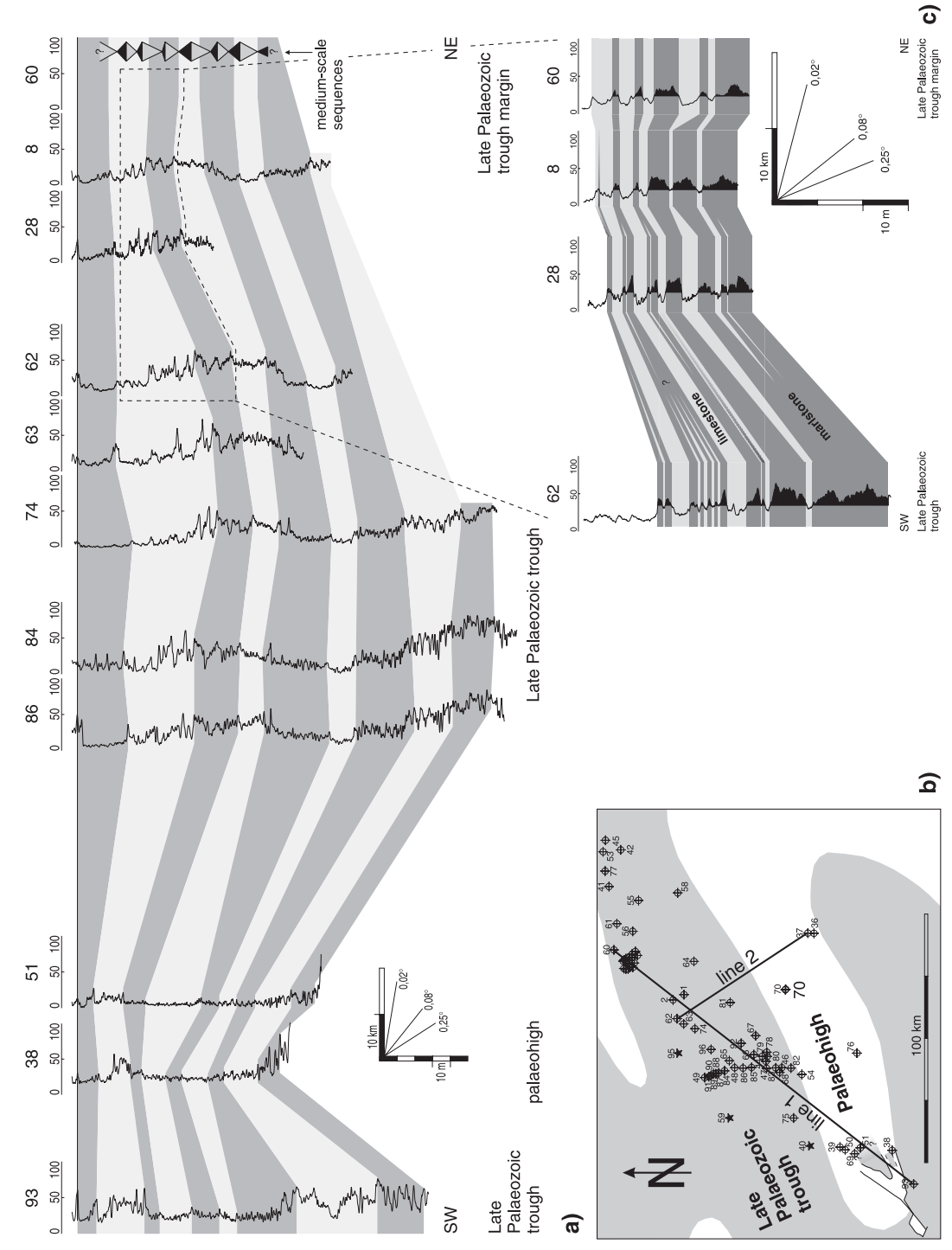
a)
b)
c)
N
Late Palaeozoic trough
Palaeohigh
line 1
line 2
70
100 km
SW
NE
Late Palaeozoic trough
palaeohigh
Late Palaeozoic trough margin
medium-scale sequences
10 km
10 m
0,02°
0,08°
0,25°
limestone
marlstone

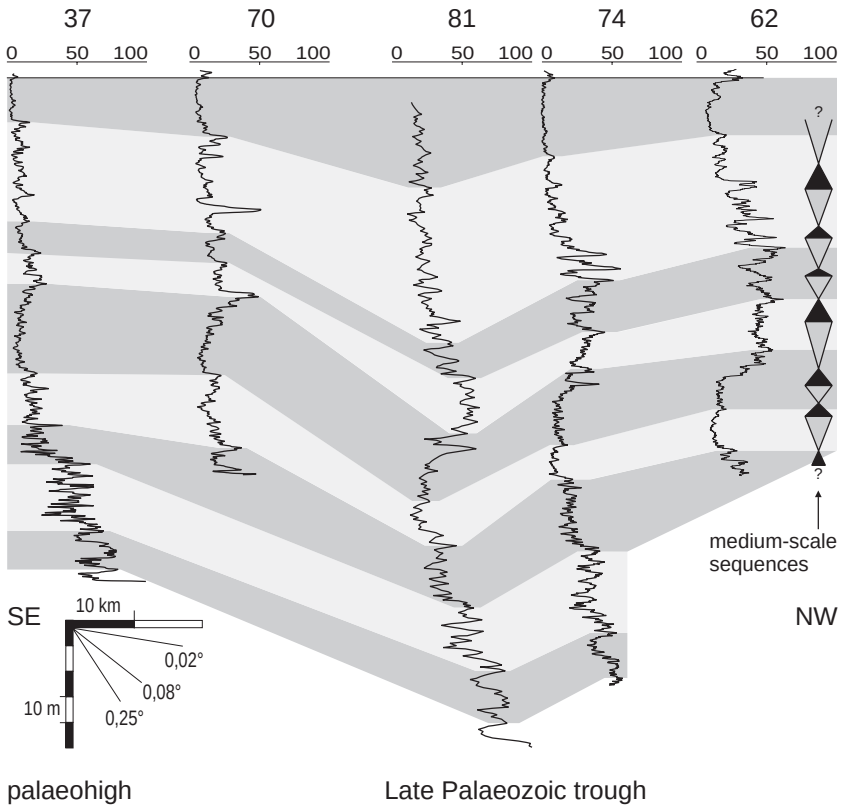

Fig. 11. Regional gamma-ray correlation (line 2 in Fig. 10b). The sediment thickness distribution is related to the underlying palaeotopography. Wells located on palaeohighs show low sediment thicknesses compared to wells located above palaeodepressions.

This model suggests that at least in periods of an overall regressive trend maximum flooding is represented on the deeper shelf by limestone beds whereas sequence boundaries are regarded to be hidden in marlstone layers. In this study, stable isotope and palynofacies evidence also suggest that the rise/fall turnaround (maximum flooding) is situated in limestone beds.

5.5. Regional correlation

5.5.1. Gamma-ray correlation

The thickness variations observed in the regional gamma-ray correlation (Figs. 10a and 11) can be related to underlying palaeotopography. Fig. 10b is a map of the distribution of the underlying Late Palaeozoic troughs for the study area according to

Fig. 10. (a) Regional gamma-ray log correlation (line 1 in b). The sediment thickness distribution is related to the underlying palaeotopography. Wells located on palaeohighs show low sediment thicknesses compared to wells located above palaeodepressions. The correlation of medium-scale sequences based only on gamma-ray logs is problematic as the turnarounds of medium-scale sequences do not always correspond to well-defined gamma-ray peaks. Instead the turnarounds are often located at some point on the rising or falling part of the gamma-ray curve and are therefore hard to pick. The reason for that is that the turnarounds of medium-scale sequences are picked at pronounced oxygen isotope and palynoclast peaks and the sample resolution of isotope and palynofacies data is considerably lower than that of the gamma-ray logs. However, the medium-scale sequences could be correlated within the time slices established by gamma-ray log correlation by means of stable isotopes. (b) Map with datapoints, correlation lines and underlying Late Palaeozoic troughs and highs (after Ziegler, 1990; Allenbach, 2001, 2002). (c) Detail of correlation line 1. The abundance of marlstone beds and the absolute content of marlstones decrease significantly in the transect from basin (thick marls) to basin margin (thin marls) suggesting a palaeotopographic control on marl deposition.

Ziegler (1990) and Allenbach (2001, 2002). Line 1 starts above a Late Palaeozoic trough in the Southwest, passes a palaeohigh and runs through another underlying Late Palaeozoic trough towards the trough margin in the NE. The distribution of Late Palaeozoic troughs is well mirrored in the sediment thickness distribution. Wells located on palaeohighs show reduced thicknesses compared to wells located inside palaeodepressions. The very sharp decrease in thickness between wells 93 and 38 is due to synsedimentary tectonics documented by Allenbach (2001, 2002). Line 2 (Fig. 11) is a SE to NW transect from palaeohigh towards palaeodepression. Again, the sediment thickness distribution is very well reflected by the distribution of pre-existing palaeorelief.

The influence of palaeotectonic structures on the distribution and facies of successive sedimentary packages has been documented elsewhere by several authors (Kassler, 1973; Purser, 1973; Alesi, 1984; Danielli, 1988; Longrace and Ginger, 1988; Wetzel et al., 1993, 2003; Lomando, 1999; Allenbach, 2001, 2002). This study implies that the Late Palaeozoic troughs and highs acted as an important controlling factor for the Mesozoic epeiric deposition. This is consistent with the observations of Wetzel et al. (2003) in northern Switzerland.

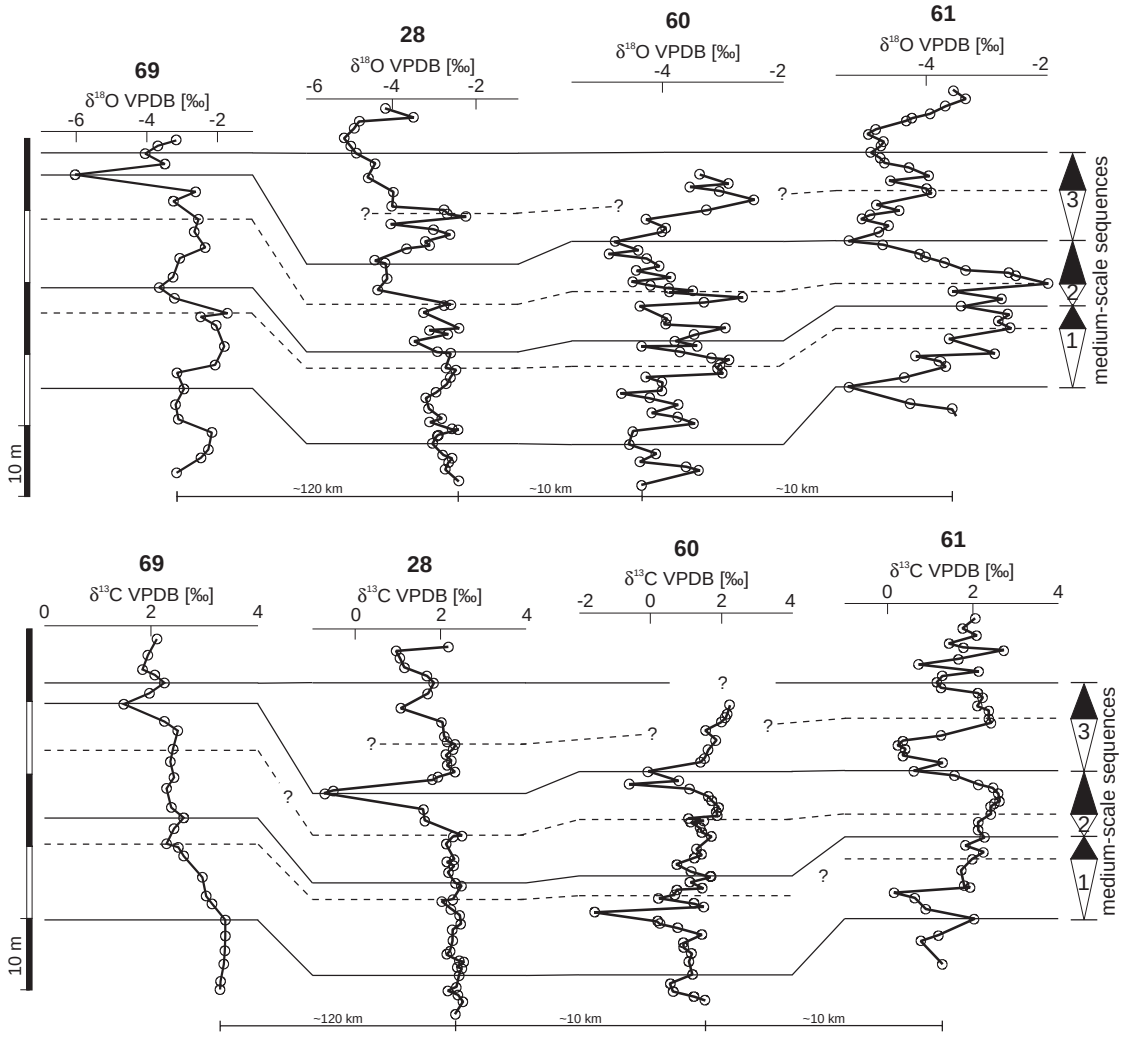

Fig. 12. Regional correlation of medium-scale sequences by carbon and oxygen isotopes.

The significant decrease in abundance of marlstone beds and in absolute marlstone content in the transect from basin to basin margin displayed in Fig. 10c seems to be also related to palaeotopography. It is likely that marlstone deposition occurred preferentially in the deeper basin in more quiet water and that individual marlstone layers pinch out when approaching the basin margin where deposition of clastic fines was obstructed by increased water energy.

5.5.2. Isotope correlation

Oxygen isotopes are sensitive to diagenesis (Veizer, 1974, 1992). However, in the present dataset a strong diagenetic overprint is unlikely because the oxygen isotope curves correlate over long distances (>100 km; Fig. 12). If any overprint has occurred, it must have been slight, preserving the original trend.

Segments of the carbon and oxygen curves corresponding to medium-scale sequences correlate regionally suggesting an allocyclic control on medium-scale sequence formation. The correlation lines may, in addition to the sequence stratigraphic units delineated and gamma-ray log correlation, therefore be used as high-resolution chemostratigraphic time lines.

6. Conclusions

1. Sequence stratigraphic patterns in mostly mud-dominated carbonates of a deeper epicontinental carbonate ramp were investigated in the Upper Jurassic of southern Germany. Facies, stable isotope and palynofacies data were integrated as sedimentological criteria alone were found to be not sufficient to establish a robust sequence stratigraphic framework.
2. Various scales of sequences could be distinguished: small-scale sequences are stacked to form medium-scale sequences, and the latter probably record 400 kyr Milankovitch signals.
3. Isotope and palynofacies analyses suggest that climatically induced sea-level fluctuations control the formation of medium-scale sequences. Rise/fall sequence turnarounds (maximum flooding) are indicated by a low absolute palynoclast abundance and a negative peak in oxygen isotopes (maximum warming). Fall/rise turnarounds are indicated by a sudden increase in absolute palynoclast abundance and a positive peak in oxygen isotopes.
4. The palynofacies and isotope peaks do not always coincide with bedding surfaces or lithologic contacts. Sequence stratigraphic boundaries such as maximum flooding or transgressive surfaces thus do not necessarily correspond to obvious and distinct stratal surfaces in these deeper ramp carbonates, but are marked by “turnaround zones”. Maximum flooding zones are located within limestone units. Marlstones are regarded as “lowstand” to early-rise deposits that cannot be differentiated.
5. The growth of deeper-water sponge/microbial bioherms is strongly controlled by nutrients and relative sea-level. Thrombolitic bioherms form during sea-level rises and decreasing nutrient availability. Thrombolitic/stromatolitic bioherms form during sea-level falls and increasing nutrient availability. Bioherm termination is due to smothering by nutrients and clastic influx.
6. Medium-scale sequences can be correlated regionally by means of gamma-ray log and stable isotope records.
7. Regional correlations revealed that sediment distribution is controlled by underlying palaeotectonic elements (Late Palaeozoic troughs and swells).

Acknowledgements

The authors would like to thank the Geological Survey of Baden-Württemberg (esp. W. Werner and M. Franz), the Deutsche Bahn AG and the Nagra (Switzerland) for making cores and gamma-ray logs available. E. Samankassou and A. Wetzel are thanked for constructive reviews of an earlier version of the manuscript. We thank the following companies for access to their quarries: Rohrbach Zement, Geisinger Kalkstein Schotterwerk and Heinz Schotterwerke. Funding for this study has been provided by the DFG (Deutsche Forschungsgemeinschaft) through a grant to T. Aigner and J. Pross (project Ai17/6).

References

Abbink O, Targarona J, Brinkhuis H, Visscher H. Late Jurassic to earliest Cretaceous palaeoclimatic evolution of the southern North Sea. Glob Planet Change 2001;30;231–56.

Alesi EJ. Der Trigonodus-Dolomit im Oberen Muschelkalk von SW-Deutschland. Arb Inst Geol Paläontol Univ Stuttg NF 1984;79;1–53.

Allenbach RP. Synsedimentary tectonics in an epicontinental sea: a new interpretaion of the Oxfordian basins of northern Switzerland. Eclogae Geol Helv 2001;94;265–87.

Allenbach RP. The ups and downs of "Tectonic Quiescence"—recognizing differential subsidence in the epicontinental sea of the Oxfordian in the Swiss Jura Mountains. Sediment Geol 2002;150;323–42.

Baier J, Schweigert G. Zum Vorkommen von Aulacostephanus yo (D'Orbigny) im Schwäbischen Jura (Ober-Kimmeridgium, SW-Deutschland). Neues Jahrb Geol Paläontol, Monatsh 2001;3; 184–92.

Bartolini A, Pittet B, Mattioli E, Hunziker JC. Shallow-platform palaeoenvironmental conditions recorded in deep-shelf sediments: C and O stable isotopes in Upper Jurassic sections of southern Germany (Oxfordian–Kimmeridgian). Sediment Geol 2003;160;107–30.

Berger WH, Vincent E. Deep-sea carbonates: reading the carbon isotope signal. Geol Rundsch 1986;75;249–69.

Bombardiere L, Gorin GE. Stratigraphical and lateral distribution of sedimentary organic matter in Upper Jurassic carbonates of SE France. Sediment Geol 2000;132;177–203.

Boulter MC, Riddick A. Classification and analysis of palynodebris from the Palaeocene sediments of the Forties field. Sedimentology 1986;33;871–86.

Braun S, Fazies-, Log- und Sequenz-Analyse im Malm gammadelta der Mittleren Schwäbischen Alb (Wiesensteig). Unpublished diploma thesis, University of Tübingen; 1999. p. 1–105.

Cole C, Harding IC. Palynofacies analysis of the Wessex Basin, Lower Jurassic. In: Underhill JR, editor. Developement, Evolution and Petroleum Geology of the Wessex Basin. Spec Publ-Geol Soc Lond, vol. 133, 1998. p. 165–85.

Colombié C. Sédimentologie, stratigraphie séquentielle et cyclostratigraphie du Kimméridgien du Jura suisse et du Bassin vocontien (France): relations plate-forme-bassin et facteurs déterminants. GeoFocus 2002;4;1–198.

Craig H. The measurement of oxygen isotope palaeotemperatures. In: Tongiorgi E, editor. Stable Isotopes in Oceanographic Studies and Palaeotemperatures. Pisa: Consiglio Nazionale delle Richerche, Laboratorio di Geologia Nucleare; 1965. p. 161–82.

Cross TA, Lessenger MA. Sediment volume partitioning: rationale for stratigraphic model evaluation and high-resolution stratigraphic correlation. Spec Publ-Nor Pet Soc 1998;8;171–96.

Danielli HM. The Eocene reservoirs of Wafra field, Kuwait/Saudi Arabia partitioned neutral zone. In: Lomando AJ, Harris PM, editors. Giant Oil and Gas Fields. SEPM Core Workshop, vol. 12; 1988. p. 119–54.

Defarge C, Trichet J, Coute A. On the appearance of cyanobacterial calcification in modern stromatolites. Sediment Geol 1994; 94;11–9.

Dromart G, Gaillard C, Jansa LF. Deep-marine microbial structures in the Upper Jurassic of Western Tethys. In: Bertrand-Sarfati J, Monty CLV, editors. Phanerozoic Stromatolites, vol. II. Berlin: Springer-Verlag; 1994. p. 295–318.

Elderfield H, Wheat CG, Mottl MJ, Monnin C, Spiro B. Fluid and geochemical transport through oceanic crust: a transect across the eastern flank of the Juan de Fuca Ridge. Earth Planet Sci Lett 1999;172;151–65.

Epstein S, Buchsbaum R, Lowenstam HA, Urey HC. Revised carbonate-water isotopic temperature scale. Geol Soc Amer Bull 1953;64;1315–26.

Golubic L, Knoll AH. Prokayotes. In: Lipps JH, editor. Fossil Prokaryotes and Protists. Boston: Blackwell; 1993. p. 51–76.

Gwinner MP. Origin of the Upper Jurassic of the Swabian Alb. Contrib Sedimentol 1976;5;1–75.

Gygi RA. Mineralostratigraphy, litho- and biostratigraphy combined in correlation of the Oxfordian (Late Jurassic) formations of the Swiss Jura range. Eclogae Geol Helv 1986; 79(2);385–454.

Gygi RA. Die Paläogeographie im Oxfordium und frühestem Kimmeridgium in der Nordschweiz. Jahresh Geol Landesamtes Baden-Württ 1990;32;207–22.

Gygi RA. Integrated stratigraphy of the Oxfordian and Kimmeridgian (Late Jurassic) in northern Switzerland and adjacent southern Germany. Mem Swiss Acad Sci 2000a;104;1–151.

Gygi RA. Annotated index of lithostratigraphic units currently used in the Upper Jurassic of northern Switzerland. Eclogae Geol Helv 2000b;93;125–46.

Hallock P, Schlager W. Nutrient excess and the demise of coral reefs and carbonate platforms. Palaios 1986;1;389–98.

Hantzpergue P, Baudin F, Mitta V, Olferiev A, Zakharov V. The Upper Jurassic of the Volga basin: ammonite biostratigraphy and occurrence of organic-carbon rich facies Correlations between boreal–subboreal and submediterranean provinces. Mém Mus Natl Hist Nat 1998;179;9–33.

Hardenbol J, Thierry J, Farley MB, Jaquin T, De Garciansky PC, Vail PR. Mesozoic and cenocoic sequence stratigraphic framework of European. In: De Garciansky PC, et al, editors. Mesozoic and Cenozoic Sequence Stratigraphy of European Basins. SEPM Spec Publ, vol. 60. 1998. p. 3–13.

Harris AJ, Tocher BA. Palaeoenvironmental analysis of Late Cretaceous dinoflagellate cyst assemblages using high resolution sample correlation from the Western Interior Basin, USA. Mar Micropaleontol 2003;48;127–48.

Herrle JO, Kößler P, Friedrich O, Erlenkeuser H, Hemleben C. High-resolution carbon isotope records of the Aptian to Lower Albian from SE France and the Mazagan Plateau (DSDP Site 545): a stratigraphic tool for paleoceanographic and paleobiologic reconstruction. Earth Planet Sci Lett 2004;218;149–61.

Homewood P, Mauriaud P, Lafont F. Best practices in sequence stratigraphy. Elf Explor Prod Mem 2000;25 [81 pp.].

Huc AY. Sedimentology of organic matter. In: Frimmel FH, Christman RF, editors. Humic Substances and Their Role in the Environment; 1988. p. 215–43.

Hug WA. Sequenzielle Faziesentwicklung der Karbonatplattform des Schweizer Jura im Späten Oxford und frühestem Kimmeridge. GeoFocus 2003;7;1–156.

Kassler P. The structural and geomorphic evolution of the Persian Gulf. In: Purser BH, editor. The Persian Gulf-Holocene Carbonate Sedimentation and Diagenesis in a Shalow Epicontinental Sea. Berlin: Springer-Verlag; 1973. p. 11–32.

Kempe S, Kazmierczak J, Reimer A, Landmann G, Reitner J. Microbialites and hydrochemistry of the Crater Lake of Satonda—a status report. Gött Arb Geol Paläontol 1996;2; 59–63.

Keupp H, Jenisch A, Herrmann R, Neuweiler F, Reitner J. Microbial carbonate crusts—a key to the environmental analysis of fossil spongiolites? Facies 1993;29;41–54.

Leinfelder RR. Upper Jurassic reef types and controlling factors—a preliminary report. Profil 1993;5;1–45.

Leinfelder RR. Jurassic reef ecosystems. In: Stanley Jr GD, editor. The History and Sedimentology of Ancient Reef Systems. New York: Kluwer Academic/Plenum Publishers; 2001. p. 251–309.

Leinfelder RR, Nose M, Schmid DU, Werner W. Microbial crusts of the Late Jurassic: composition, palaeoecological significance and importance in reef construction. Facies 1993;29; 195–230.

Leinfelder RR, Krautter M, Laternser R, Nose M, Schmid DU, Schweigert G, et al. The origin of Jurassic reefs: current research developments and results. Facies 1994;31;1–56.

Leinfelder RR, Werner W, Nose M, Schmid DU, Krautter M, Laternser R, et al. Paleoecology, growth parameters and dynamics of coral, sponge and microbolite reefs from the late Jurassic. Gött Arb Geol Paläontol 1996;2;227–48.

Lomando AJ. Structural influences on facies trends of carbonate inner ramp systems, examples from the Kuwait–Saudi Arabian coast of the Arabian Gulf and Northern Yucatan, Mexico. GeoArabia 1999;4;339–60.

Longrace SA, Ginger EP. Evolution of the lower Cretaceous Ratawi Oolite reservoir, Wafra field, Kuwait–Saudi Arabia partitioned neutral zone. In: Lomando AJ, Harris PM, editors. Giant Oil and Gas Fields. SEPM Core Workshop, vol. 12. 1988. p. 273–331.

Marshall JD. Climatic and oceanographic isotopic signals from the carbonate record and their preservation. Geol Mag 1992;129; 143–60.

McCarthy FMG, Gostlin KE, Mudie PJ, Pedersen RO. The palynological record of terrigenous flux to the deep sea: late Pliocene–Recent examples from 41°N in the abyssal Atlantic and Pacific oceans. Rev Palaeobot Palynol 2004;128;81–95.

Meyer RKF, Schmidt-Kaler H. Paläogeographischer Atlas des süddeutschen Oberjura (Malm). Geol Jahrb, A 1989;115;3–77.

Meyer RKF, Schmidt-Kaler H. Paläogeographie und Schwammriffentwicklung des süddeutschen Malm—ein Überblick. Facies 1990;23;175–84.

Mitchum RM, Vail PR, Thompson S. Seismic stratigraphy and global changes of sea-level Part 2: the depositional sequence as a basic unit for stratigraphic analysis. In: Payton CE, editor. Seismic Stratigraphy—Applications to Hydrocarbon Exploration. Memoir - American Association of Petroleum Geologists, vol. 26. 1977. p. 53–62.

Munnecke A, Westphal H. Shallow-water aragonite recorded in bundles of limestone–marl alternations—the Upper Jurassic of SW Germany. Sediment Geol 2004;164;191–202.

Padden M, Weissert H, Funk H, Schneider S, Gansner C. Late Jurassic evolution and carbon-isotope stratigraphy of the western Tethys. Eclogae Geol Helv 2002;95;333–46.

Pawellek T. Fazies-, Sequenz-, und Gamma-ray-Analyse im höheren Malm der Schwäbischen Alb (SW-Deutschland). Tüb Geowiss Arb, A Geol Paläontol Stratigr 2001;61;1–246.

Pawellek T, Aigner T. Fazies, Petrophysik und Rohstoffeigenschaften von Karbonatgesteinen des Schwäbischen Oberjura—ein Atlas. Jahresber Mitt Oberrhein Geol Ver NF 2002;84; 257–321.

Pawellek T, Aigner T. Stratigraphic architecture and gamma ray logs of deeper ramp carbonates (Upper Jurassic, SW Germany). Sediment Geol 2003a;159;203–40.

Pawellek T, Aigner T. Apparently homogenous "reef"-limestones built by high-frequency cycles: upper Jurassic, SW-Germany. Sediment Geol 2003b;160;259–84.

Pittet B, Mattioli E. The carbonate signal and calcareous nannofossil distribution in an Upper Jurassic section (Balingen-Tieringen, Late Oxfordian, southern Germany). Palaeogeogr Palaeoclimatol Palaeoecol 2002;179;71–96.

Pittet B, Strasser A. Depositional sequences in deep-shelf environments formed through carbonate-mud import from the shallow platform (Late Oxfordian, German Swabian Alb and eastern Swiss Jura). Eclogae Geol Helv 1998;91;149–69.

Pittet B, Strasser A, Mattioli E. Depositional sequences in deep-shelf environments: a response to sea-level changes and shallow-platform carbonate productivity (Oxfordian, Germany and Spain). J Sediment Res 2000;10(2);392–407.

Pross J. Paleo-oxygenation in Tertiary epeiric seas: evidence from dinoflagellate cysts. Palaeogeogr Palaeoclimatol Palaeoecol 2001;166;369–81.

Purser BH. Sedimentation around Bathymetric Highs in the Southern Persian Gulf. In: Purser BH, editor. The Persian Gulf—Holocene Carbonate Sedimentation and Diagenesis in a Shalow Epicontinental Sea. Berlin: Springer-Verlag; 1973. p. 157–77.

Quenstedt FA. Der Jura; 842 S. Tübingen: Laupp und Siebeck; 1858.

Rehfeld U. Mediating and limitating processes during the development of spongiolitic bioconstructions in Jurassic and Cretaceous strata—a paleontological, facial and geochemical analysis. Gött Arb Geol Paläontol 1996;2;249–58.

Ricken W. Epicontinental marl–linestone alternations: event deposition and diagenetic bedding (Upper Jurassic, southwest Germany). In: Bayer U, Seilacher A, editors. Sedimentary and Evolutionary Cycles. Lecture Notes in Earth Sciences, vol. 1. 1985. p. 127–62.

Ruf M, Aigner T. Facies and poroperm characteristics of a carbonate shoal (Muschelkalk, South German Basin): a reservoir analogue investigation. J Pet Geol 2004;27(3);215–39.

Sandberg P. An oscillating trend in Phanerozoic non-skeletal carbonate mineralogy. Nature 1983;305;19–22.

Schmid DU. Marine Mikrobolithe und Mikroinkrustierer aus dem Oberjura. Profil 1996;9;101–251.

Schweigert G. Immigration of Amoeboceratids into the Submediterranean Upper Jurassic of SW Germany. GeoRes Forum 2000;6;203–10.

Sharland PR, Archer R, Casey DM, Davies RB, Hall SH, Heward AP, et al. Arabian plate sequence stratigraphy. GeoArabia Special Publication, vol. 2. Bahrain: Gulf PetroLink; 2001.

Sonnenfeld MD. Sequence evolution and hierarchy within the lower Mississippian Madison limestone in Wyoming. In: Longman MW, Sonnenfeld MD, editors. Paleozoic Systems of the Rocky Mountain Section; 1996. SEPM. p. 165–92.

Strasser A, Hillgärtner H, Hug W, Pittet B. Third-order depositional sequences reflecting Milankovitch cyclicity. Terra Nova 2000; 12;303–11.

Stockmarr J. Tablets with spores used in absolute pollen analysis. Pollen Spores 1971;13;615–21.

Taylor SP, Sellwood BW. The context of lowstand events in the Kimmeridgian (Late Jurassic) sequence stratigraphic evolution of the Wessex–Weald Basin, Southern England. Sediment Geol 2002;151;89–106.

Taylor SP, Sellwood BW, Gallois RW, Chambers MH. A sequence stratigraphy of the Kimmeridgian and Bolonian stages (late Jurassic): Wessex–Weald Basin, southern England. J Geol Soc 2001;158;179–92.

Tyson RV, Follows B. Palynofacies prediction of distance from sediment source: a case study from the Upper Cretaceaous of the Pyrenees. Geology 2000;28;569–71.

Valdes PJ. Atmospheric general circulation models of the Jurassic. Philos Trans R Soc Lond, B 1993;341;317–26.

Valdes PJ, Sellwood BW. A palaeoclimate model for the Kimmeridgian. Palaeogeogr Palaeoclimatol Palaeoecol 1992;95;47–72.

Valdes PJ, Sellwood BW, Price GD. Modelling Late Jurassic Milankovitch climate variations. In: House MR, Gale AS, editors. Orbital Forcing Timescales and Cyclostratigraphy. Special Publication-Geological Society of London, vol. 85. 1995. p. 115–32.

Van Wagoner JC, Posamentier HW, Mitchum RM, Vail PR, Sarg JF, Loutit TS, et al. An overview of the fundamentals of sequence stratigraphy and key definitions. In: Wilgus CK, Hastings BS, Kendall CG, St C, Posamentier HW, Ross CA, Van Wagoner JC, editors. Sea Level Changes: An Integrated Approach. SEPM Spec Publ, vol. 42. 1988. p. 39–45.

Van Wagoner JC, Mitchum RM, Campion KM, Rahmanian VD. Siliciclastic sequence stratigraphy in well logs, cores and outcrop: concepts for high resolution correlation of time and facies. AAPG Methods Explor Ser 1990;7;55.

Veizer J. Chemical diagenesis of belemnite shells and possible consequences for paleotemperature determinations. Neues Jahrb Geol Paläontol Abh 1974;147;91–111.

Veizer J. Depositional and diagenetic history of limestones: stable and radiogenic isotopes. In: Clauer N, Chaudhuri S, editors. Isotopic Signatures and Sedimentary Records. Lecture Notes in Earth Sciences, vol. 43. Berlin: Springer-Verlag; 1992. p. 13–48.

Waterhouse H. High-resolution palynofacies investigation of Kimmeridgian sedimentary cycles. In: House MR, Gale AS, editors. Orbital Forcing Timescales and Cyclostratigraphy. Geological Society Special Publication, vol. 85. 1995. p. 75–114.

Waterhouse H. Orbital forcing of palynofacies in the Jurassic of France and the United Kingdom. Geology 1999;27;511–4.

Weissert H, Erba E. Volcanism, CO_2 and palaeoclimate: a Late Jurassic–Early Cretaceous carbon and oxygen isotope record. J Geol Soc (Lond) 2004;161;695–702.

Weissert H, Lini L, Föllmi KB, Kuhn O. Correlation of Early Cretaceous carbon isotope stratigraphy and platform drowning events: a possible link? Palaeogeogr Palaeoclimatol Palaeoecol 1998;137;189–203.

Wetzel A, Allia V, Gonzales R, Jordan P. Sedimentation und Tektonik im Ostjura. Eclogae Geol Helv 1993;86;313–32.

Wetzel A, Allenbach R, Allia V. Reactivated basement structures affecting the sedimentary facies in tectonically "quiescent" epicontinental basin: an example form NW Switzerland. Sediment Geol 2003;157;153–72.

Whalen T, Day J, Eberli GP, Homewood PW. Microbial carbonates as indicators of environmental change and biotic crisis in carbonate systems: examples from the Late Devonian, Alberta basin, Canada. Palaeogeogr Palaeoclimatol Palaeoecol 2002; 181;127–51.

Wheeler HE. Baselevel, lithosphere surface and time stratigraphy. GSA Bull 1964;75;599–610.

Whitaker MF. The Usage of Palynostratigraphy and Palynofacies in Definition of Troll Field Geology. Norwegian Petroleum Consultants A/S; 1984.

Wood R. Are reefs and mudmounds really so different? Sediment Geol 2001;145;161–71.

Wood GD, Gabriel AM, Lawson JC. Palynological techniques—processing and microscopy. In: Jansonius J, McGregor DC, editors. Palynology: Principles and Applications. AASP, vol. 1. 1996. p. 29–50.

Ziegler B. The "White" (Upper) Jurassic in Southern Germany. Stuttg Beitr Naturkd, B 1977;26;1–79.

Ziegler PA. Geological Atlas of Western and Central Europe. 2nd ed. The Hague: Shell; 1990.